Estimating Network Parameters From Combined Dynamics of Firing Rate and Irregularity of Single Neurons

Kosuke Hamaguchi, Alexa Riehle and Nicolas Brunel

J Neurophysiol 105:487-500, 2011. First published 18 August 2010; doi:10.1152/jn.00858.2009

You might find this additional info useful...

Supplemental material for this article can be found at:
http://jn.physiology.org/content/suppl/2010/12/07/jn.00858.2009.DC1.html

This article cites 52 articles, 27 of which can be accessed free at:
http://jn.physiology.org/content/105/1/487.full.html#ref-list-1

Updated information and services including high resolution figures, can be found at:
http://jn.physiology.org/content/105/1/487.full.html

Additional material and information about ***Journal of Neurophysiology*** can be found at:
http://www.the-aps.org/publications/jn

This infomation is current as of May 24, 2011.

Journal of Neurophysiology publishes original articles on the function of the nervous system. It is published 12 times a year (monthly) by the American Physiological Society, 9650 Rockville Pike, Bethesda MD 20814-3991. Copyright © 2011 by the American Physiological Society. ISSN: 0022-3077, ESSN: 1522-1598. Visit our website at http://www.the-aps.org/.

Downloaded from jn.physiology.org on May 24, 2011

J Neurophysiol 105: 487–500, 2011.
First published August 18, 2010; doi:10.1152/jn.00858.2009.

Estimating Network Parameters From Combined Dynamics of Firing Rate and Irregularity of Single Neurons

Kosuke Hamaguchi,[1,2,3] Alexa Riehle,[4] and Nicolas Brunel[2,3]

[1]*Amari Research Unit, RIKEN, Brain Science Institute, Saitama, Japan;* [2]*Université Paris Descartes, Laboratoire de Neurophysique et Physiologie, Paris, France;* [3]*Centre National de la Recherche Scientifique (CNRS), Unité Mixte de Recherche (UMR) 8119, Paris, France; and* [4]*Institut de Neurosciences Cognitives de la Méditerranée, UMR 6193, CNRS, Université Aix-Marseille 2, Marseille, France*

Submitted 22 September 2009; accepted in final form 13 August 2010

Hamaguchi K, Riehle A, Brunel N. Estimating network parameters from combined dynamics of firing rate and irregularity of single neurons. *J Neurophysiol* 105: 487–500, 2011. First published August 18, 2010; doi:10.1152/jn.00858.2009. High firing irregularity is a hallmark of cortical neurons in vivo, and modeling studies suggest a balance of excitation and inhibition is necessary to explain this high irregularity. Such a balance must be generated, at least partly, from local interconnected networks of excitatory and inhibitory neurons, but the details of the local network structure are largely unknown. The dynamics of the neural activity depends on the local network structure; this in turn suggests the possibility of estimating network structure from the dynamics of the firing statistics. Here we report a new method to estimate properties of the local cortical network from the instantaneous firing rate and irregularity (CV_2) under the assumption that recorded neurons are a part of a randomly connected sparse network. The firing irregularity, measured in monkey motor cortex, exhibits two features; many neurons show relatively stable firing irregularity in time and across different task conditions; the time-averaged CV_2 is widely distributed from quasi-regular to irregular (CV_2 = 0.3–1.0). For each recorded neuron, we estimate the three parameters of a local network [balance of local excitation-inhibition, number of recurrent connections per neuron, and excitatory postsynaptic potential (EPSP) size] that best describe the dynamics of the measured firing rates and irregularities. Our analysis shows that optimal parameter sets form a two-dimensional manifold in the three-dimensional parameter space that is confined for most of the neurons to the inhibition-dominated region. High irregularity neurons tend to be more strongly connected to the local network, either in terms of larger EPSP and inhibitory PSP size or larger number of recurrent connections, compared with the low irregularity neurons, for a given excitatory/inhibitory balance. Incorporating either synaptic short-term depression or conductance-based synapses leads many low CV_2 neurons to move to the excitation-dominated region as well as to an increase of EPSP size.

INTRODUCTION

Firing properties of single neurons are determined both by intrinsic membrane characteristics and by their connectivity matrix within their local network. Whereas the electrical properties of a neuronal membrane are rather well understood (Hodgkin and Huxley 1952; Koch 1999), it is currently impossible to obtain the full connectivity matrix of a local network in the cortex. Even if the connectivity matrix of a specific area of a neural tissue could be obtained experimentally, it would still be desirable to represent it in the form of a set of probabilistic or descriptive rules to provide a clear insight of the network architecture. In any case, it is of interest to devise a method that provides information about the relationship between the parameters defining the connectivity and the recorded activity of neurons.

Cortical neurons have been described to have a firing irregularity close to a Poisson process (Compte et al. 2003; Shinomoto et al. 2003; Softky and Koch 1993; but see Maimon and Assad 2009; Shinomoto et al. 2009). Several theoretical studies have argued that a balance of excitation and inhibition can explain this high irregularity (Amit and Brunel 1997; Brunel 2000; Burkitt 2001; Gerstein and Mandelbrot 1964; Shadlen and Newsome 1998; Tsodyks and Sejnowski 1995; van Vreeswijk and Sompolinsky 1996). More recently, direct measurements of conductance changes during UP states in vitro and in vivo have revealed proportional changes of excitatory and inhibitory conductances (Haider et al. 2006; Shu et al. 2003). These lines of evidence support the balanced network hypothesis in which excitatory and inhibitory inputs to neurons are balanced. This balance should be, at least in part, generated by local connectivity of the cerebral cortex, but the properties of this connectivity are not fully understood yet.

Some of the previously mentioned theoretical papers derived the statistics of firing (firing rate, firing irregularities) of single neurons in a network as a function of the parameters defining network connectivity (Brunel 2000; Burkitt 2001). In this paper, we propose to investigate the reverse relationship: estimate parameters of the local circuit of a given neuron from its statistics of firing as obtained from extracellular electrophysiological recordings. The problem of finding local network parameters from the firing statistics is an inverse problem, and it is difficult to solve it in general. From theoretical and simulation studies of leaky integrate-and-fire (LIF) neurons, it is known that the balance between excitation and inhibition is a crucial parameter that determines the behavior of firing rate and firing irregularity (see e.g., Brunel 2000; Shadlen and Koch 1998). If a network is purely driven by excitatory inputs, the firing irregularity typically decreases as the firing rate increases (Fig. 1*B*). However, if the recurrent inhibition is balanced with or even dominates excitation, firing irregularity tends to be stable and decoupled from the firing rate changes (Fig. 1*C*). Such a weak modulation of the firing irregularity is also observed in vivo, in area MT and V1 (Shimokawa and Shinomoto 2009). Motivated by these findings, we set out to statistically estimate the parameter regions that can best explain the observed dynamics of the firing rate and irregularity. The method we propose here relies on the instantaneous measure of the firing rate ν and an instantaneous measure of the

Address for reprint requests and other correspondence: N. Brunel, Université Paris Descartes, CNRS. UMR 8119, 75270 Paris Cedex 06, France (E-mail: nicolas.brunel@parisdescartes.fr).

0022-3077/11 Copyright © 2011 The American Physiological Society

Downloaded from jn.physiology.org on May 24, 2011

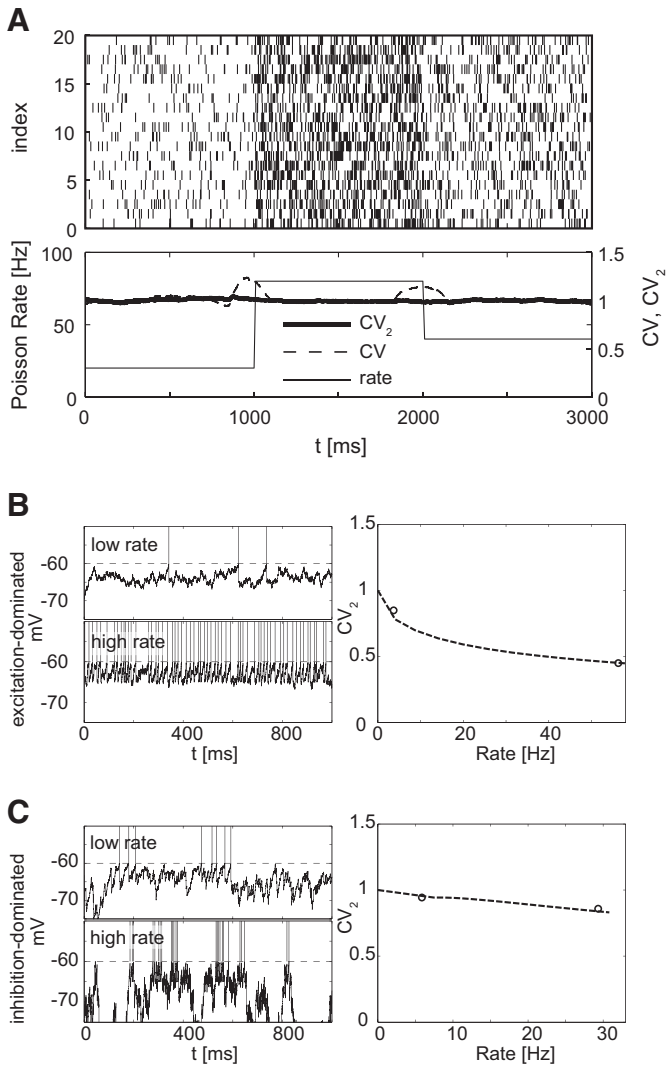

FIG. 1. *A, top*: a spike raster plot of rate-modulated Poisson spike train the firing rate of which changes at $t = 1{,}000$ and 2,000 ms. *Bottom*: CV (dashed line) is more susceptible to the rate modulation than CV_2 (thick solid line). The firing rate of the Poisson spike train is shown by the thin solid line. The firing irregularity should ideally be flat, but CV has an upward bias when rate changes. Each measure is calculated within a 300 ms sliding window across 500 trials. *B*: firing irregularity drops as the firing rate increases in a network driven by excitatory synapses only, but remains to be high in an inhibition-dominated network. *Left*: 2 examples of the simulated membrane potential dynamics of a leaky integrate-and-fire (LIF) neuron in low and high firing rate regime. *Right*: the theoretical relationship between rate and CV_2. Simulation results are shown in circles. The parameters are $\tau = 30$ ms, $\tau_{ref} = 2$ ms, $C_E = 100$, delay $= 0.5$ ms, $N = 10{,}000$, $V_{th} = -50$ mV, $V_{reset} = -55$ mV, $V_L = -60$ mV, $J_{ext} = 0.8$, $J = 0$, and $g = 0$. *C*: firing irregularity is relatively constant in an inhibition-dominated network. Parameters are the same as in *B* except for $J = J_{ext} = 0.3$, and $g = 7$.

firing irregularity, such as the CV_2 metric (Holt et al. 1996) as a function of time. This method is composed of the following three steps. *1*) Recording and analysis: the instantaneous firing rate and the instantaneous firing irregularity are measured within a sliding window of duration ΔT ms. The firing irregularity is measured by the metric CV_2 and compared with the theory. *2*) Theory: given a particular single neuron model and a model of its local network, we predict how the output firing rate ν and the CV_2 depend on the external input, either numerically or analytically. Changes in external inputs lead to changes in single neuron firing statistics (ν, CV_2) and draw a trajectory in $\nu - CV_2$ plane. This trajectory depends strongly on network parameters, such as the ones that control the balance between excitation and inhibition (Fig. 1, *B* and *C*). *3*) Fitting the model to the data: we calculate the distance (cost function) between the experimental data points obtained from the electrophysiological recordings and the model trajectory in the $\nu - CV_2$ plane. The best fit parameters are searched. We numerically searched the global minima in a discretized parameter space.

We applied this strategy to the spike data of single neurons recorded from the motor cortex of two behaving Rhesus monkeys as described in Roux et al. (2003, 2006). Analysis of these recordings reveals that firing irregularity is relatively weakly modulated in time compared with the firing rate, and its time average over the task period is nearly independent from task conditions, such as the direction of the arm movement. The distribution of CV_2s over the population ranges from 0.3 to >1 and is possibly bimodal, which is suggested by previous results from other cortical areas (Shinomoto et al. 2003, 2009). We then attempted to extract some information about parameters of the local circuits of the primary motor cortex. Our parameter estimation method suggests the following. *1*) Irregular spiking neurons operate in balanced or inhibition-dominated network. *2*) Quasi-regular spiking neurons can operate in an excitation-dominated region if the number of recurrent connections per neurons is very small (~10), but as the recurrent connectivity increases, the ratio of excitation-inhibition shifts to an inhibition-dominated region. *3*) The estimated excitatory postsynaptic potential (EPSP) sizes and the ratio or inhibitory PSP (IPSP)/EPSP of irregular spiking neurons are larger than those of quasi-regular neurons if the number of presynaptic neurons is the same. As the number of local connections per neuron increases, the estimated EPSP size becomes smaller. *4*) Incorporating either synaptic short-term depression or conductance-based synapses leads to a large number of neurons (especially low irregularity neurons) to move to the excitation-dominated region and to an increase in EPSP amplitudes. Preliminary results were presented in an abstract (Hamaguchi et al. 2008).

METHODS

Electrophysiology and tasks

Data for this analysis were obtained from two earlier studies (Roux et al. 2003, 2006). Two male Rhesus monkeys participated in this study (data from *monkey R* are partly described in Roux et al. 2003), and single neuron spiking data from *monkey O* were recorded on the same electrodes with the local field potentials (LFPs) as described in Roux et al. (2006). Detailed descriptions of the experimental techniques were described in Roux et al. (2003, 2006). Care and treatment of the animals during all stages of the experiments conformed to the European and French government regulations.

EXPERIMENTAL TASKS. The two monkeys were trained to perform two types of tasks: a choice-reaction time task (chRT) and a self-paced movement task (Self). In front of the monkey, a vertical panel with three touch-sensitive light-emitting diodes was set. The diodes were horizontally aligned. First, the center diode was lit in yellow. The monkey had to touch it to initiate the trial. Then the following two tasks were randomly performed in blocks:

CHOICE-REACTION TASK (chRT). After a fixed delay (500 ms), the two peripheral diodes were lit simultaneously as the preparatory

Downloaded from jn.physiology.org on May 24, 2011

signal (PS), one in red and the other in green. The position of the color was randomly chosen. An auditory, directionally noninformative signal followed after either a short or a long delay as the response signal (RS). If the RS occurred after a short delay, the monkey had to touch the red diode, and if it occurred after a long delay, the green one should be touched. ($n = 89$ neurons; *monkey O*: $n = 58$, *monkey R*: $n = 31$).

SELF-PACED MOVEMENT TASK (SELF). After a fixed delay (500 ms), only one of the two peripheral diodes was lit in red or green as PS. The position and color were randomly chosen. In this task, there was no response signal, and the monkey had to initiate the movements by himself. If the color was red, the monkey had to initiate the movement after a correctly estimated short delay. For the green diode, the monkey had to initiate the movement after a long delay. ($n = 75$ neurons; *monkey O*: $n = 42$, *monkey R*: $n = 33$).

In both chRT and Self tasks, same delay conditions were used, but the values of the delays were different for the two monkeys. In *monkey O,* two combinations of delays were used: 600–1,200 and 1,000−1,400 ms (Roux et al. 2006) and in *monkey R* only 600–1,200 ms (Roux et al. 2003), for the short and long delays, respectively. A trial was considered as correct when the movement was performed to the correct target and initiated within a temporal window of 300 ms starting at the end of the delay. Otherwise, that trial was classified as an error trial and was not rewarded. We analyzed only successful trials in this paper. For each task, movement onset (MVT) was defined when the hand releases the center yellow diode, and we aligned the time axis of each trial to the MVT.

To record extracellularly multiple single-neuron activities, a multielectrode, computer-controlled microdrive (*monkey R*: Reitboeck system, Thomas Recording, Giessen, Germany; *monkey O*: MT-EPS, AlphaOmega, Nazareth, Israel) was used to transdurally insert up to seven microelectrodes (*monkey R*: quartz insulated platinum-tungsten electrodes, 80 μm OD, impedance:: 2–5 MΩ at 1,000 Hz; *monkey O*: epoxy insulated tungsten electrodes, Frederick Haer, 0.5–1.2 MΩ at 1,000 Hz). The inter-electrode distance was between 230 and 700 μm; however, because the electrodes were driven independently from each other, their distance in depth may have varied for each recording. From each electrode, electrical signals were amplified with a gain of 5,000 to 10,000 (MCP+, AlphaOmega) and high-pass filtered by using in-house hardware (active filtering) at 300 Hz for selecting action potentials (spikes). Spikes of only one single neuron per electrode were then isolated by using a window discriminator in *monkey R* or between one and three neurons per electrode (although rarely >2 were discriminated in practice) by using on-line spike sorting with a template matching algorithm (MSD, AlphaOmega) in *monkey O*. Sorted spike data along with behavioral events (occurrences of signals and performance of the animal) were stored for off-line analysis with a time resolution of 1 kHz.

Irregularity measures

Several measures of spike time irregularity have been proposed so far in different contexts. The most widely used measure, the coefficient of variation (CV) of interspike intervals (Softky and Koch 1993), is defined as

$$\mathrm{CV} = \frac{\sqrt{\langle (\mathrm{ISI} - \langle \mathrm{ISI} \rangle)^2 \rangle}}{\langle \mathrm{ISI} \rangle} \quad (1)$$

where ISI is an interspike interval, $\langle x \rangle$ is the sample average of x. The CV is equal to 1 for a stationary Poisson spike train and takes values of 0 for a completely regular spike train. If the spike train is not stationary, i.e., the firing rate changes in time, the CV tends to overestimate the irregularity of the underlying process (Nawrot et al. 2008). For example, if the firing rate of a Poisson spike train changes in time, the CV computed from finite time windows becomes >1 around the time of the firing rate changes (Fig. 1*A*). Several alternative measures of firing irregularity that are more robust to rate modulations have been proposed recently: CV_2 (Holt et al. 1996), LV (Shinomoto et al. 2005), IR (Davies et al. 2006), SI (Miura et al. 2006), and CV in operational time (Nawrot et al. 2008). CV_2, LV, IR, and SI are calculated based on neighboring ISIs, and they become zero for completely regular spike trains. According to their original definition, only CV_2 and LV take values of 1 for a Poisson spike train, but IR and SI can also be normalized such as to be unity for the Poisson case.

In this paper, we have chosen the CV_2 (Holt et al. 1996) as a local measure of spike time irregularity because it provides a less biased estimate of irregularity for a small, finite sample size (Ponce-Alvarez et al. 2010). For a more detailed comparison of these measures and their performance, see Ponce-Alvarez et al. (2010). The CV_2 is computed in the following equations

$$\mathrm{ISI}_k = t_k - t_{k-1} \quad (2)$$

$$\mathrm{CV}_2^{(k)} = \frac{2\left|\mathrm{ISI}_{k+1} - \mathrm{ISI}_k\right|}{\mathrm{ISI}_{k+1} + \mathrm{ISI}_k} \quad (3)$$

$$\langle \mathrm{CV}_2 \rangle = \frac{1}{K}\sum_{k=1}^{K} \mathrm{CV}_2^{(k)} \quad (4)$$

where t_k is the kth spike from a cell and $CV_2{}^{(k)}$ is the value of the CV_2 assigned to the kth spike.

Data analysis

We calculated instantaneous firing rate, ν (t), the instantaneous firing irregularity $CV_2(t)$ (Holt et al. 1996), and their SEs [$\sigma_n(t)$, $\sigma_{CV2}(t)$] as a function of time, using a sliding window. The instantaneous firing rate at time t, $\nu(t)$, is calculated by taking the number of spikes divided by the length of the sliding window around time t, including all trials. The SE of the firing rate $\sigma_n(t)$ is the intertrial SD of the firing rate divided by the square root of the number of trials.

The instantaneous firing irregularity at time t is calculated as follows: a $CV_2{}^{(k)}$ value calculated from the preceding and the following ISIs is assigned to kth spike in the sliding window (Fig. 2*A*), using *Eq. 3*. The first and last spikes of each trial are not taken into account in the analysis because they do not have preceding or following ISIs. The instantaneous firing irregularity $CV_2(t)$ is the mean of $CV_2{}^{(k)}$ values within a sliding window averaged over all the trials (*Eq. 4*). The SE of $CV_2(t)$, $\sigma_{CV2}(t)$, is defined as the SD of $CV_2{}^{(k)}$ values within the sliding window over the trials, divided by square root of the number of spikes. Here we approximated the distribution of the sample mean of $CV_2{}^{(k)}$ as a Gaussian distribution.

Whereas the use of the CV_2 measure provides a much more robust way of assessing single neuron irregularity than the CV measure, we have noticed two issues on the use of CV_2. One is the validity of the Gaussian approximation of the sample mean of CV_2 that determines the confidence limit of CV_2 in our paper. The other is the bias toward higher values during epochs of transient very low-firing rate; even though CV_2 is less susceptible to the changes of firing rate compared with CV, there is still a bias in CV_2 estimates when the firing rate changes abruptly especially when firing rate drops off to near zero rate. We now address these two issues.

CONFIDENCE LIMIT OF CV_2. The first question is how to determine the confidence limits of the measured $CV_2(t)$ values. From the central limit theorem, the distribution of the sample mean from independently and identically distributed variables converges to Gaussian. Once a sample mean is obtained, the true mean is expected to be distributed according to a t-distribution around the sample mean. The t-distribution also converges to a Gaussian for large sample sizes. For CV_2 measures, however, two neighboring CV_2 values are correlated due to the shared ISI, and the average of the correlated variables does not generally converge to its true mean even for large sample sizes. To

Downloaded from jn.physiology.org on May 24, 2011

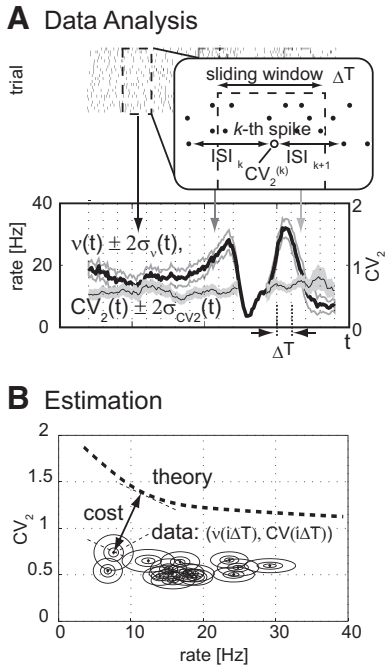

FIG. 2. A schematic picture of the data analysis and parameter estimation. *A*: data analysis part: the instantaneous firing rate with 2 SE region, $\nu(t) \pm 2\sigma_n(t)$ [$\nu(t)$: thick line, $\sigma_n(t)$: gray lines] and the instantaneous firing irregularity with 2 SE region, $CV_2(t) \pm 2\sigma_{CV2}(t)$ [$CV_2(t)$: thin line, $\sigma_{CV2}(t)$: shaded region] are calculated in sliding windows with a length of $\Delta T = 100$ ms. The details of these calculations are given in the supplementary materials (Supplementary Figs. S1–S2). The removed data in the middle of the time course are due to the bias-suppression method to avoid low confidence region of the data [see the supplementary materials (Supplementary Fig. S3)]. Down-sampled data at time points of [brace]ΔT, $2\Delta T$, $3\Delta T$, . . . } are passed to the parameter estimation process. *B*: parameter estimation: for each experimental data sample [$\nu(i\Delta T)$,$CV_2(i\Delta T)$], a projection point on the theoretical line (dashed line) is calculated for a given parameter set in a metric space with each axis normalized by their SD {$\sigma_n(i\Delta T)$, $\sigma_{CV2}(i\Delta T)$}. A set of parameters that minimizes a cost function (sum of minimum distances from data to a theoretical line) is searched.

remove the effect of within sample correlation, one can average every other CV_2 value, but this down-sampling may increase the estimation error of the true CV_2 value. To study the properties of CV_2 statistics, we numerically computed the distribution of sample means of CV_2 from a gamma distributed ISI and confirmed that averaging all CV_2 values actually yields to lower SE than taking every other CV_2 value (Supplementary Fig. S1*B*),[1] and that the assumption of the Gaussian distribution of the sample mean of CV_2 is valid if there are large numbers of samples (Supplementary Fig. S2). The details of how to obtain confidence limits of the CV_2 statistics are given in the supplementary materials. We set the threshold to 20 spike counts per sliding window above which we can safely approximate the sample mean distribution as Gaussian. We define a data point as the couple of {$\nu(t)$, $CV_2(t)$} calculated within one sliding window around time t. The data points containing <20 spike counts are not used in the parameter estimation part, and are not presented in the figures.

SUPPRESSING THE BIAS TOWARD HIGH CV_2. The second question is how to suppress the upward bias of estimated CV_2s observed at abrupt firing rate changes. We find that the spikes that are nearest neighbors in a time window with low spike counts tend to have high CV_2 values when this time window follows and/or precedes windows with much larger spike counts. This is caused by the abnormally long ISIs in this low-firing rate region. One way to correct this overestimation error is to remove spikes at the border of low to high spike count (see also Davies et al. 2006). This bias-suppression method is very effective and drastically reduces the overestimation error (Supplementary Fig. S3). The details of the bias-suppression method are described in the supplementary materials. The threshold of low to high spike count was set to 20 spike counts within the sliding window over trials. After applying this bias-suppression method, the firing irregularity at time t, $CV_2(t)$, is calculated as the average of $CV_2^{(k)}$ within the sliding window, including all trials.

To summarize, the firing irregularity is calculated as follows: after applying the bias-suppression method described in the preceding text, the $CV_2(t)$ and $\sigma_{cv2}(t)$ are calculated as the sample mean and conventional SE from the $CV_2^{(k)}$ values within the sliding window over all the trials. The removal of spikes in the bias-suppression method is only applied to the CV_2 statistics, and the firing rates are not affected.

In this paper, we used $\Delta T = 100$ ms time window, and data were always aligned to MVT. Only spikes occurring during periods from MVT −1,100 to MVT +300 ms, for short delay trials and MVT −1,500 to MVT +300 ms, for long delay trials were taken into account. There are four conditions (short or long delays and left or right arm movements) for each of the two types of tasks (chRT and Self). Therefore the activity of one neuron can be recorded in eight different conditions at most. We do not focus on the description of the neural representation of the movement or the stimuli but only on an estimation of the parameters of the local network in which each neuron is embedded. We treat each condition independently and estimate the network parameters for each condition separately. In the parameter estimation part, we analytically calculate the CV_2 of the LIF neuron model driven by a white noise (Brunel 2000; Siegert 1951; Tuckwell 1988) by using numerical inverse Laplace transform of the analytically obtained ISI distribution in the frequency domain.

Neuron and network model

We consider a sparsely and randomly connected network of LIF neurons (Amit and Brunel 1997; Brunel 2000) (Fig. 3) as a model of a local cortical circuit in the primary motor cortex that is activated during the arm-reaching task. The membrane potential dynamics of neuron i ($i = \{1, 2, \ldots, N\}$) is described as follows

$$C dV_i/dt = -g_L(V_i - V_L) + I_i(t) \quad (5)$$

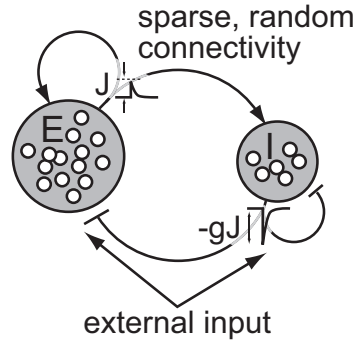

FIG. 3. Network structure: Neurons are sparsely and randomly connected. Here, J is the excitatory postsynaptic potential (EPSP) size, $-gJ$ is the inhibitory PSP (IPSP) size. The other network parameters are as follows; $\beta = 1/4$ is the ratio of thumber of excitatory neuron and inhibitory neuron. C_E is the number of recurrent excitatory presynaptic neurons per neuron from the local cortical circuit, and $C_I = \beta C_E$ is that of inhibitory presynaptic neurons per neuron.

[1] The online version of this article contains supplemental data.

Downloaded from jn.physiology.org on May 24, 2011

$$I_i(t) = C\sum_{j=1}^{N} J_{ij}\sum_k \delta(t - t_j^k - D) \quad (6)$$

where C is the membrane capacitance, g_L is the leak conductance, V_L is the leak voltage, and D is the synaptic conduction delay. When $V_i > V_L$, the ith neuron emits a spike and V_i is reset to V_r and fixed during the absolute refractory period τ_{ref}. The synaptic efficacy, J_{ij} is defined as $J_{ij} = J$ if the synapse is excitatory, or $J_{ij} = -gJ$ if the synapse is inhibitory. Each neuron also receives excitatory inputs from external populations. We referred to a set of neurons in other areas of the brain that project their axons to the local network as the external population. The synaptic efficacy is $J_{ij} = J_{ext}$ where the jth neuron is now in an external population. For simplicity, we set $J_{ext} = J$ in this paper. In this model, the synaptic current is described as an instantaneous current (δ-function).

The whole network is composed of $N_E = 0.8N$ excitatory neurons and $N_I = 0.2N$ inhibitory neurons, making the ratio of the excitatory and inhibitory neuron, $\beta = N_I/N_E = 0.25$. We also set the number of recurrent, excitatory (inhibitory) presynaptic neurons per postsynaptic neuron as C_E ($C_I = \beta C_E$).

Self-consistent analysis of firing rate and CV

For simplicity, we assume homogeneous neuron properties for both excitatory and inhibitory neurons. Because the connectivity is the same for both neuron types, the statistical properties of the inputs are the same. As a result, both neuron types have the same firing rate. Assuming that the correlations in the inputs to different neurons in the network can be neglected, and the jump of EPSP(IPSP) is much smaller than the distance to the threshold, then one can rewrite the input of *Eq. 6* by using a diffusion approximation (Amit and Brunel 1997; Brunel 2000)

$$I_i(t) = \mu(t) + \sqrt{\tau_m}\sigma(t)\mathrm{d}W_i \quad (7)$$

where $\tau_m = C/g_L$ is the membrane time constant, $\langle \mathrm{d}W_i(t)\rangle = 0$ and $\langle \mathrm{d}W_i(t)\mathrm{d}W_j(t')\rangle = \delta_{ij}\delta(t - t')$. The mean input $\mu(t)$ is given as

$$\mu(t) = \mu_l(t) + \mu_{ext}(t) \quad (8)$$

$$\mu_l(t) = \tau_m J C_E(1 - g\beta)\nu(t) \quad (9)$$

$$\mu_{ext}(t) = \tau_m J_{ext} C_{ext}\nu_{ext}(t) \quad (10)$$

where $\mu_l(t)$ is the average input from local connections and $\mu_{ext}(t)$ is the average input from outside of the network. The firing rate $\nu(t)$ is the measured spike emission rate, representing the firing rate of the local cortical circuits. We will use measured firing rate as $\nu(t)$. The number of afferent connections from the external population to the network is C_{ext}. The firing rate of the external population is ν_{ext}. The variance of the input $\sigma^2(t)$ is

$$\sigma^2(t) = \sigma^2_l(t) + \sigma^2_{ext}(t) \quad (11)$$

$$\sigma^2_l(t) = \tau_m J^2 C_E(1 + g^2\beta)\nu(t) \quad (12)$$

$$\sigma^2_{ext}(t) = \tau_m J^2 C_{ext}\nu_{ext}(t) \quad (13)$$

This procedure is the so-called "mean-field" approximation. It means that the local cortical circuit we consider now is described by the mean-firing rate $\nu(t)$. Note that ν_{ext} enter the equations only as a product of C_{ext} and ν_{ext}. Therefore there is only a single variable describing the total external input rate—the sum of all firing rates of the external neurons projecting to the neurons the spikes of which we are measuring. Therefore from now on, we simply describe $C_{ext}\nu_{ext}$ as ν'_{ext}.

To calculate the firing rate and CV_2 of the local network, we assume that within the sliding window, a network state is very close to the stationary state (quasi-stationarity). This assumption becomes valid if the time scale of the firing rate change is much longer than the membrane time constant. The quasi-stationary firing rate and the CV_2 value can be calculated by the following procedure: solving the self-consistent equation of the firing rate (Amit and Brunel 1997; Brunel 2000), numerically calculating the ISI distribution by using the inverse Laplace transform of the analytical expression of the ISI distribution in the frequency domain (Sugiyama et al. 1970), and computing the mean of the CV_2 values.

The self-consistent equation of the firing rate can be obtained by solving the following equation

$$\nu - f(\nu, \nu'_{ext}, \Pi) = 0 \quad (14)$$

where f is the transfer function indicating the output firing rate of a LIF neuron as a function of ν, ν'_{ext}, and Π, and given as

$$f(\nu, \nu'_{ext}, \Pi) = \left[\tau_{ref} + \tau\sqrt{\pi}\int_{y_r}^{y_{th}} \mathrm{d}y \exp(y^2)(1 + \mathrm{erf}(y))\right]^{-1} \quad (15)$$

where $y_{th} = (V_{th} - E_{syn})/\sigma$ and $y_r = (V_r - E_{syn})/\sigma$, $E_{syn} = V_L + \mu$, $\tau = \tau_m$. Note that μ and σ given in *Eqs. 8* and *11* are the functions of firing rates ν, ν'_{ext} and network parameters Π. The error function, $\mathrm{erf}(x)$ is defined as $\mathrm{erf}(x) = 2/\sqrt{\pi}\int_0^x \mathrm{d}x\exp(-x^2)$. To explicitly show that the solution of *Eq. 14* is determined by external population rate ν'_{ext} and network parameters Π, we denote the solution of *Eq. 14* as

$$\nu^* = \phi(\nu'_{ext}, \Pi) \quad (16)$$

To obtain CV_2, we first calculate the ISI distribution from the numerical inversion of the analytical expression of the ISI distribution in the frequency domain (Sugiyama et al. 1970). The analytical expression of the ISI distribution in the frequency domain is

$$p_{ISI}(\omega|y_{th}, y_r) = U(\omega, y_r)/U(\omega, y_{th}) \quad (17)$$

where $p_{ISI}(\omega|y_{th}, y_r)$ is the Laplace transform of the ISI distribution for a given stationary Gaussian noise input of mean μ and SD σ. $U(\omega,y)$ is the combination of confluent hypergeometric functions (Brunel 2000)

$$U(\omega, y) = \sqrt{\pi}/\Gamma\big((1 + w\tau)/2\big)M\big((1 - w\tau)/2, 0.5, -y^2\big) + 2y\sqrt{\pi}/\Gamma(w\tau/2)M(1 - w\tau/2, 1.5, -y^2) \quad (18)$$

where $M(\lambda, a, b)$ is the confluent hypergeometric function of the first kind (see Abramovicz and Stegun 1970). Note that the ISI distribution $p_{ISI}(t \mid y_{th}, y_r)$ depends only on mean input μ and SD σ, but μ and σ are actually functions of the external firing rate ν'_{ext}, the firing rate ν^*, and the network parameters Π. Therefore we first solve the *Eq. 16* to obtain ν^* for computing μ and σ, and then we compute $p_{ISI}(t \mid y_{th}, y_r)$. From this, we calculate CV_2 from the numerical integration of the following equation

$$CV_2^* = \int_0^\infty\int_0^\infty \mathrm{d}t_1\mathrm{d}t_2\, p(t_1|y_{th}, y_r)p(t_2|y_{th}, y_r)2|t_1 - t_2|/(t_1 + t_2 + 2\tau_{ref}) \quad (19)$$

To explicitly show that CV_2 is a function of the network parameters and the external input, we denote $CV_2^* = \psi(\nu'_{ext}, \Pi)$.

Now the single neuron parameters describing single neurons are τ_m, τ_{ref}, D, V_L, V_{th}, V_r, while network parameters are g, J, C_E, and ν'_{ext} ($= C_{ext}\nu_{ext}$). Single neuron parameters are taken from La Camera et al. (2006) and Rauch et al. (2003) where the parameters of a single LIF neuron were fitted from the response of pyramidal cells to a noisy current injection. Here we set $\tau_m = 30$ ms, $\tau_{ref} = 2$ ms, $V_{th} = -50$ mV, $V_{reset} = -55$ mV, and $V_L = -60$ mV. Now the remaining free parameters are g, J, C_E, and ν'_{ext}. From now on, we denote a set of network parameters to be estimated as $\Pi = \{J, g, C_E\}$. The external firing rate ν_{ext} is also one of the parameters controlling the activity, but this parameter can dynamically change during the task. We therefore left ν'_{ext} as a dynamical variable and will not estimate it as a fixed parameter. In fact, we can marginalize the likelihood of Π by the probability $p(\nu'_{ext})$.

Downloaded from jn.physiology.org on May 24, 2011

Theory for estimating network parameters from single neuron statistics

The next step is to search for the network parameters that best describe the data. For a given data set ($\nu(t_i)$, $CV_2(t_i)$), we want to maximize a posterior probability $P(\Pi|\{\nu, CV_2\})$ where $\Pi = \{J, C_E, g\}$ is a set of the network parameters. From the Bayes rule, the posterior is

$$p(\Pi|\{\nu, CV_2\}) = \frac{p(\{\nu, CV_2\}|\Pi)}{p(\{\nu, CV_2\})} p(\Pi) \propto p(\{\nu, CV_2\}|\Pi) p(\Pi) \quad (20)$$

From now on, we assume the uninformative prior $p(\Pi) = c$ (constant) within the searched parameter ranges to avoid making bias in the estimation of the network parameters. By choosing the sampling time t_i to be integer multiples of the sliding window size $\Delta T = 100$ ms, we can neglect the correlation within the sample mean of rate $\{\nu(t_i)\}$ and within the sample mean of firing irregularity $\{CV_2(t_i)\}$ where $t_i = i\Delta T$ and $i = \{1, 2, \ldots\}$. Then we can decouple the probability $p(\{\nu, CV_2\}|\Pi)$ into the product of $p[\nu(t_i), CV_2(t_i)|\Pi]$. Next we assume that the estimation errors made on $\nu(t_i)$ and $CV_2(t_i)$ are approximately independent. As a consequence, we can decouple $p[\nu(t_i), CV_2(t_i)|\Pi]$ into $p[\nu(t_i)|\Pi]\, p[CV_2(t_i)|\Pi]$. Now the probability distribution $p(\{\nu, CV_2\}|\Pi)$ can be decomposed into the products of the independent distributions of $p[\nu(t_i)|\Pi]$ and $p[CV_2(t_i)|\Pi]$. Then, the posterior distribution is

$$p(\Pi|\{\nu, CV_2\}) \propto \Pi_{i=1}^{n} p(\{\nu(t_i), CV_2(t_i)\}|\Pi) p(\Pi) \quad (21)$$

$$p(\{\nu(t_i), CV_2(t_i)\}|\Pi) = \int d\nu'_{ext} \exp\left(-\frac{(\nu(t_i) - \phi(\nu'_{ext}, \Pi))^2}{2\sigma_\nu(t_i)^2}\right) \times \exp\left(-\frac{(CV_2(t_i) - \psi(\nu'_{ext}, \Pi))^2}{2\sigma_{CV_2}(t_i)^2}\right) p(\nu'_{ext}) \quad (22)$$

where $\sigma_\nu(t_i)$ and $\sigma_{CV2}(t_i)$ are SE of the rate and CV_2 defined at time t_i. By using the saddle-point approximation (Daniels 1980) and taking log of posterior, we can approximate the log-posterior as

$$\log p(\{\nu(t_i), CV_2(t_i)\}|\Pi) \approx -\frac{(\nu(t_i) - \phi(\nu^*_{ext}, \Pi))^2}{2\sigma_\nu(t_i)^2} - \frac{(CV_2(t_i) - \psi(\nu^*_{ext}, \Pi))^2}{2\sigma_{CV_2}(t_i)^2} \quad (23)$$

where ν'_{ext} gives the minimum of *Eq. 23*. Here we assumed an uninformative prior for ν_{ext}. Intuitively, the saddle-point approximation is equivalent to search for the closest point between $[\nu(t_i), CV(t_i)]$ and a point on a theoretical curve $[\phi(\nu_{ext}, \Pi), \psi(\nu_{ext}, \Pi)$; Fig. 2*B*]. The distances are normalized by $\sigma_n(t_i)$ and $\sigma_{CV2}(t_i)$ for each data point. Therefore the cost for the parameter Π is

$$\text{cost}(\Pi) = -\sum_i \log p(\{\nu(t_i), CV_2(t_i)\}|\Pi) \quad (24)$$

Once the cost-function has been defined, the best-fit parameters can be searched by several numerical methods, such as the gradient-descent method. In our case, however, the landscape of the cost is very flat in large parameter regions, and the gradient-descent search methods are neither efficient nor practical. Therefore we calculated the cost-function for the entire discretized space of network parameters to find the global minimum or minima. In this paper, we used the discretization of $C_E = [10, 100, 1{,}000]$, $g = [0, 0.25, 0.5, \ldots, 8]$, and $J = [0.01, 0.02, \ldots, 0.39, 0.40, 0.50, 0.60, \ldots, 0.90, 1.00]$. Because we have used a limited parameter range, this can be viewed as a prior distribution of the parameter space. For example, EPSPs size <0.01 mV are not considered here because such values are far smaller than the noise level in intracellular recordings. The performance of the estimation depends on the number of data points and their distribution over the $\nu - CV_2$ plane. The larger the number of data points $\{\nu(t_i), CV(t_i)\}$ and the wider their distribution in the rate $-$ CV_2 space, the better we can estimate the network parameters. Therefore we choose neurons and task conditions which have ≥ 10 data points, and the difference between the minimum and maximum of the firing rate is ≥ 10 Hz. The number of trials is >30 [$n = 507$ conditions (*monkey O*: $n = 303$, *monkey R*: $n = 204$) from $n = 164$ neurons (*monkey O*: $n = 100$, *monkey R*: $n = 64$)].

Synaptic properties

To investigate how the choice of the model, such as synaptic properties, affects the estimate of network parameters, we also used other models with synapses with short-term depression (STD) and conductance-based synapses and separately estimated the network parameters in these two cases.

SHORT-TERM DEPRESSION. STD is a major feature of synapses between cortical pyramidal cells (e.g., Varela et al. 1997). A simple phenomenological model has been developed by Tsodyks and Markram (1997) that provided a very good fit of their data. In the STD synapse model, the EPSP size J_{ij} in *Eq. 6* is replaced by a dynamical variable that obeys

$$J_{ij} \rightarrow J_{ij} u x_j(t) \quad (25)$$

$$\tau_{STD} dx_j/dt = 1 - x - \tau_{STD} u x_j(t) \sum_k \delta(t - t_j^k - D) \quad (26)$$

where $x_j(t)$ is the fraction of vesicles available at time t, and $u\, x_j(t)$ is the fraction of vesicles released by a single action potential. $x_j(t)$ decreases by a factor $u\, x_j$ at each spike and recovers exponentially with the time constant τ_{STD}. Only excitatory synapses (both external and recurrent) are modeled according to *Eqs. 25* and *26*, while inhibitory synapses are kept fixed. We used $u = 0.5$, $\tau_{STD} = 500$ ms. The STD level of afferent synapses now depends on the external input rate ν_{ext}, thus the number of afferent synapses C_{ext} needs to be explicitly modeled here. Here we assumed that each neuron receives same number of afferent and recurrent excitatory synapses ($C_{ext} = C_E$,) (see e.g., Braitenberg and Schüz 1998). To analyze the network steady states in the presence of STD, we use the results of Romani et al. (2006). We first calculate the moments of x in a stationary state by using Laplace transform of the ISIs $p_{ISI}(w|y_{th}, y_r)$

$$<x> = [1 - p_{ISI}(1/\tau_{STD}|y_{th}, y_r)\kappa]/[1 - (1 - U)p_{ISI}(1/\tau_{STD}|y_{th}, y_r)\kappa] \quad (27)$$

$$<x^2> = \{1 - 2(1 - (1 - U) < x >) p_{ISI}(1/\tau_{STD}|y_{th}, y_r)\kappa + (1 - 2(1 - U) < x >) p_{ISI}(2/\tau_{STD}|y_{th}, y_r)\kappa^2\}/[1 - (1 - U)^2 p_{ISI}(2/\tau_{STD}|y_{th}, y_r)\kappa^2] \quad (28)$$

$$\kappa = \exp(-\tau_{ref}/\tau_{STD}) \quad (29)$$

Then, the following parameters are used in *Eq. 15* to calculate the stationary firing rate

$$E_{syn} = V_L + \tau_m J C_E (u < x > - g\beta)\nu + \tau_m J C_E u < x_{ext} > \nu_{ext} \quad (30)$$

$$\sigma^2 = \tau_m (J^2 C_E (u^2 < x^2 > + g^2\beta)\nu + J^2 C_E u^2 < x^2_{ext} > \nu_{ext}) \quad (31)$$

where $\langle x_{ext} \rangle$ is the average fraction of vesicles available for a Poisson firing neuron at ν_{ext} Hz and is obtained by using $p_{ISI}(n/\tau_{STD}) = \nu_{ext}/(\nu_{ext} + n/\tau_{STD})$ in *Eqs. 27* and *28*.

CONDUCTANCE-BASED SYNAPSES. We have also investigated a network with conductance-based synapses. In the conductance-based synapse model, the PSP size J_{ij} in *Eq. 6* is replaced by

$$J_{ij} = a_{E/I}(V_i - V_{E/I}) \quad (32)$$

where $a_{E/I}$ is a nondimensional parameter (ratio between synaptic conductance and leak conductance) that control the size of excitatory (a_E) or inhibitory (a_I) postsynaptic potentials, and $V_{E/I}$ are the excitatory (V_E) or inhibitory (V_I) reversal potentials. Here we used $V_E =$

Downloaded from jn.physiology.org on May 24, 2011

0 mV, $V_I = -70$ mV. We calculate the stationary firing rate of the LIF network with the conductance based synapses by using the effective time constant approximation (Meffin et al. 2004). The following parameters are used in *Eq. 15*

$$\tau^{-1} = \tau_m^{-1} + (a_E C_E + a_I C_I)\nu + a_E C_{ext}\nu_{ext} \quad (33)$$

$$E_{syn} = \tau(V_L/\tau_m + (a_E C_E V_E + a_I C_I V_I)\nu + a_E C_{ext} V_E \nu_{ext}) \quad (34)$$

$$\sigma^2 = \tau\{[a_E^2 C_E (E_{syn} - V_E)^2 + a_I^2 C_I (E_{syn} - V_I)^2]\nu + a_E^2 C_{ext}(E_{syn} - V_E)^2 \nu_{ext}\} \quad (35)$$

RESULTS

Here we propose a novel method to estimate parameters of a local network in which a neuron is embedded, from the combined dynamics of firing rate and firing irregularity. Our method is valid if both the rate and the firing irregularity can be regarded as quasi-stationary within the sliding window for each sampling time t_i. We apply this method to the single-neuron spike data recorded in the motor cortex of two behaving monkeys (*monkey O*, $n = 100$ neurons; *monkey R*, $n = 64$ neurons). First, we analyze the properties the firing irregularity of our spike trains. This analysis reveals two features of the spiking activity in our set of motor cortical neurons: many neurons show temporally stable firing irregularity; the firing irregularity over the population of neurons, as measured using CV_2, are widely distributed from 0.3 to 1. Second, we estimate the network parameters from the dynamics of rate and firing irregularities. For most analyzed neurons (78.5%), the dynamics of rate and irregularity is consistent with the neuron being part of an inhibition-dominated network.

Firing properties of neurons

To study how the firing rate and the firing irregularity change during the task, their means are measured within sliding windows. For the firing irregularities, spike trains are preprocessed with the bias-suppression method; sliding windows which contain <20 spikes are discarded and not used for the data analysis (see METHODS). Figure 4*A* shows a typical example of the dynamics of rate and firing irregularity of a single neuron recorded in *monkey O* during all successful trials in one behavioral condition. Figure 4*A, top,* shows the spike raster plot aligned to MVT. Both mean firing rate and CV_2 are presented in Fig. 4*A, bottom*. The firing rate (thick solid line) clearly shows a ramping up activity preceding and following movement onset. On the other hand, the firing irregularity does not seem to change much, and the temporal modulation of CV_2 (thin solid line) does not strongly deviate from the confidence limit of $2\sigma_{CV2}$ region (shaded region). To compare the significance of the change level, we computed the psychophysical measure d' (Green and Swets 1966) of the highest and lowest value of the rate and the CV_2, where $d' = |x_H - x_L|/[\mathrm{var}(x_H) + \mathrm{var}(x_L)]^{1/2}$. Here $x_{H(L)}$ is equivalent to the highest (lowest) value of $\nu(t)$ or $CV_2(t)$ in each trial, and window. $\mathrm{var}(x_{H(L)})$ is the trial-to-trial variance of the firing rate and CV_2 within the 100 ms window around the highest (lowest) value. The larger d', the better one can discriminate the membership of a sample, i.e., whether a sample of mean rate (or mean CV_2) is derived from the lowest or highest value group. Figure 4*B* shows the histogram of d' for the firing rate (solid line) and the CV_2 (dashed line) for all task conditions and neurons recorded from both monkeys. For most of the neurons, the d' for the firing rate is higher than that for the CV_2. This indicates that most of the neurons show large firing rate changes, but the firing irregularity is rather weakly modulated.

BROAD DISTRIBUTION OF CV_2. Figure 4*E* shows the distribution of mean CV_2 values averaged over four behavioral conditions across the population of neurons of the two monkeys ($n = 164$). Spike irregularities are widely distributed from quasi-regular ($CV_2 \sim 0.3$) to highly irregular ($CV_2 > 1$). This holds true for the distribution of each monkey. In all recorded neurons, mean CV_2 values are essentially independent of task conditions (Fig. 4*C*). Neurons recorded in different tasks also showed very similar values of firing irregularity in different tasks (Fig. 4*D*). Hence each neuron seems to be characterized by a CV_2 value that is independent on the context of the task.

A possible explanation for the wide distribution of CV_2s is that distinct neuron classes (e.g., fast spiking interneurons and pyramidal neurons) could have different CV_2 distributions. Because these neuron types are expected to have also distinct mean rates, we investigated the correlation between mean firing rate and firing irregularity across neurons. A rate-CV_2 scatter plot is shown in Fig. 4*F*. Each point represents for a single neuron an average of time-averaged firing rate and CV_2 from four task conditions. The correlation coefficient is 0.05, and the least squared error fit gives $CV_2 = 0.7 + 0.001\nu$. This indicates that in a population of neurons there is negligible correlation between the mean values of firing rate and CV_2.

Estimating network parameters

In this section, we estimated the network parameters that can describe the observed dynamics of firing rate and firing irregularity. Basic assumptions are as follows; quasi-stationarity of the spike statistics during the sliding window (100 ms), the network is a sparse, randomly connected network of excitatory and inhibitory neurons; and neurons can be described as LIF neurons. The third assumption is justified by previous studies that have shown that an input-output relationship of neocortical neurons can well be described as LIF neurons (Arsiero et al. 2007; La Camera et al. 2006; Rauch et al. 2003) even though additional parameters such as adaptation improve the fitting. Here we use the standard current-based LIF model and fixed the single neuron model parameters as described in METHODS.

The random, sparsely connected network is characterized by three parameters. *1*) The inhibition/excitation balance g (IPSP/EPSP amplitude ratio). When $g = 4 = 1/\beta$, it gives the exact balance between the local, recurrent excitatory and inhibitory inputs, because we have assumed the ratio of the total number of excitatory and inhibitory neurons in a local network is 1/4. *2*) The EPSP amplitude J in mV. *3*) The number of recurrent excitatory connections per neuron C_E (the number of recurrent inhibitory synapses per neuron $C_I = \beta C_E$ is always proportional to C_E).

A typical example of the estimated parameters and of the activity of a neuron exhibiting a high firing irregularity ($CV_2 > 0.9$) is shown in Fig. 5*A*. Figure 5*A, top,* shows the dynamics of firing rate and firing irregularity. Figure 5*A, bottom,* shows the distribution of data points in the ν-CV_2 plane. Contour plots (circles) around the data points represent error bars of [0.5, 1, 2] SE. The theoretical prediction lines from the esti-

Downloaded from jn.physiology.org on May 24, 2011

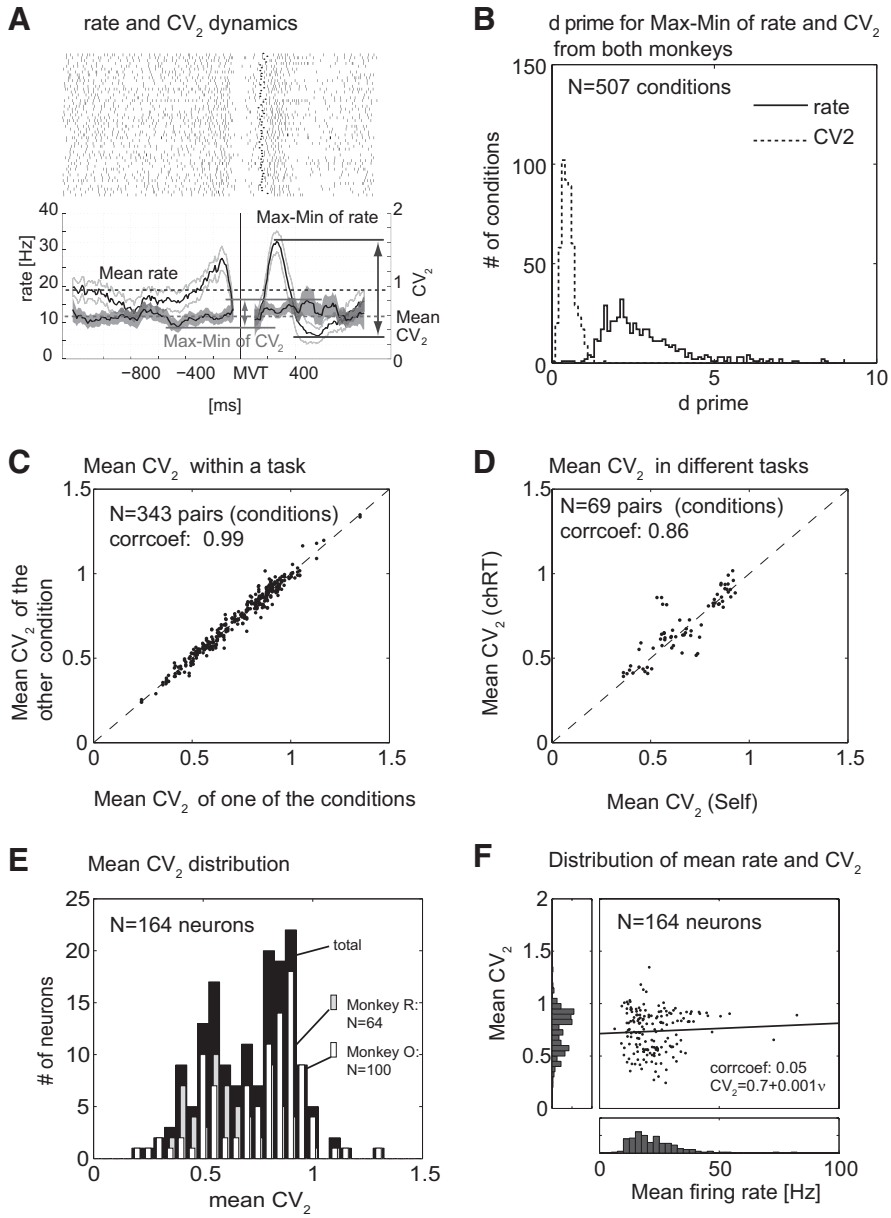

FIG. 4. *A*: dynamics of rate and firing irregularity of a neuron recorded in the motor cortex of *monkey O* during 1 trial type of the choice-reaction time task. The threshold of the spike count within a sliding window is 20. The firing rate shows significant modulation during the task, but only little the firing irregularity. The difference between the maximum and the minimum values that is used in the analysis of d' is also shown. The temporal and trial average of the firing rate and CV_2 values are also shown in dashed line. *B*: the psychophysical measure d' was used for both firing rate and CV_2 to compare the statistical significance of their highest and lowest values during the task. The histogram of d' for all task conditions and neurons shows that many neurons show a significantly large firing rate modulation but a relatively small number of neurons show a significant CV_2 change [$n = 507$ in all conditions, (*monkey O*: $n = 303$, *monkey R*: $n = 204$)]. *C*: mean CV_2 values from a single neuron show similar values in different conditions, such as the direction of arm movement and delay period. Mean CV_2 values of 1 of the 4 conditions vs. the other 3 conditions are plotted. ($n = 343$ pairs of conditions from both monkeys.) *D*: mean CV_2 shows similar values in different tasks, self-paced movement task (self) and choice-reaction time task (chRT). Mean CV_2 values during self vs. chRT tasks are shown ($n = 69$ pairs). *E*: the broad distribution of the firing irregularity over the entire population shows a diversity of neurons [$n = 164$ neurons (*monkey O*: $n = 100$, *monkey R*: $n = 64$)]. Each CV_2 value in the histogram is the averaged CV_2 over time and 4 conditions of each neuron. *F*: the correlation between the mean firing rate and the mean firing irregularity CV_2 was not significant. Each point represents a single cell's mean firing rate and CV_2 averaged over time and task conditions.

mated parameters are also overlaid. We estimated the network parameters for this neuron by using the method described in *Theory for estimating network parameters from single neuron statistics.* The estimated parameter that gives the global minimum of cost is (g, J, C_E) = (6.9, 0.27, 100) (thick gray line, cost per data: 1.343). However, we noticed that very different parameters also give very similar cost values, such as (g, J, C_E) = (5.8, 0.1, 1000) (dashed line, cost per data point: 1.345), (g, J, C_E) = (7.2, 0.8, 10) (dash-dotted line, cost per data point: 1.346) as shown in Fig. 5*A*. These parameter sets show similar cost values and the predicted theoretical lines are almost identical. This indicates that there are wide regions in parameter space that produce an essentially undistinguishable firing behavior. In other words, the firing rate-irregularity relationship is redundantly represented in the parameters of g, J, C_E.

Another typical example of neurons exhibiting quasi-regular spike trains ($CV_2 < 0.6$) is shown in Fig. 5*B*. The estimated parameter that gives the global minimum is (g, J, C_E) = (5.4, 0.03, 1,000) (thick gray line, cost per data: 0.636). However, we also found that other parameters, e.g., (g, J, C_E) = (6.0, 0.08, 100), (dashed line, cost per data: 0.660) and (g, J, C_E) = (8.0, 0.1, 10), (dash-dotted line, cost per data: 0.714), also show a very similar firing rate-irregularity relationship. The parameter space is also degenerate in low CV_2 neurons.

STRUCTURE OF THE SPACE OF PARAMETERS THAT MINIMIZES THE COST FUNCTION. Why can more than one parameter set generate similar firing rate-CV_2 dynamics? How are these parameters related to each other? To understand these questions, we studied the constraints on the parameters that can generate similar output firing statistics. The firing statistics in our model depends on mean μ and SD σ of the inputs to the neuron. We therefore ask the question, what are the network parameters that can generate given values of μ and σ? To answer this question, we rewrite *Eqs. 8* and *11* as

$$\mu = \tau J[\nu'_{ext} + C_E \nu(1 - g\beta)] \quad (36)$$

Downloaded from jn.physiology.org on May 24, 2011

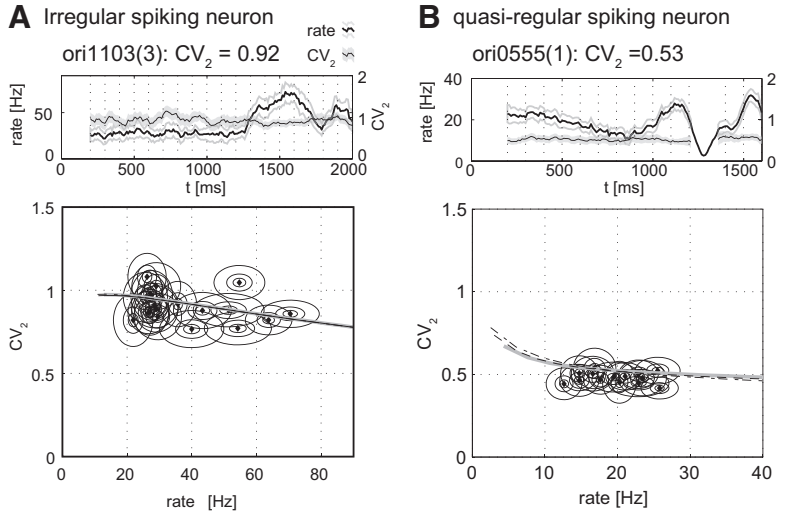

FIG. 5. Examples of the estimated parameters for an irregular and a quasi-regular spiking neuron. *A*: irregular spiking neuron. Irregularity is close to Poisson (CV = 0.92) and temporally stable. The best estimated parameter is (g, J, C_E) = (6.9, 0.27, 100) (thick gray line, costs per data point is 1.343), but the other parameters can also show a similar firing rate-irregularity relationship such as (g, J, C_E) = (5.8, 0.1, 1,000) (dashed line, cost per data point is 1.345), and (7.2 0.8, 10) (dash-dotted line, cost per data point is 1.346). *B*: quasi-regular spiking neuron. Firing irregularity is CV_2 = 0.53 and temporally stable. The best estimated parameter is (g, J, C_E) = (5.4, 0.03, 1,000) (thick gray line, cost per data point is 0.636), but the other parameters can also show a similar firing rate-irregularity relationship such as (g, J, C_E) = (6.0, 0.08, 100), (dashed line, cost per data point is 0.660), and (8.0, 0.17, 10) (dash-dotted line, cost per data point is 0.713).

$$\sigma^2 = \tau J^2[\nu'_{\text{ext}} + C_E\nu(1 - g^2\beta)] \quad (37)$$

If we assume the number of connections per neurons C_E is large, then to get a finite variance we need the EPSP amplitude J to scale roughly as $1/\sqrt{C_E}$ (van Vreeswijk and Sompolinsky 1996, 1998). Then to get a finite mean we need total excitatory and inhibitory inputs to roughly balance. Balancing excitatory and inhibitory inputs is only possible if the IPSP amplitude is strong enough

$$g > 1/\beta \quad (38)$$

In our paper, $g > 4$ because we set $\beta = 0.25$. This provides a first constraint on parameter space. This "balance" condition leads to the equation $\nu'_{\text{ext}} = C_E\nu(g\beta - 1)$. Inserting this expression in *Eq. 37*, we find the following relationship between the input variance σ^2 and the firing rate ν

$$\sigma^2 = A\nu \quad (39)$$

$$A = \tau J^2 C_E g\beta(1 + g) \quad (40)$$

These simple arguments therefore predict there should be an (approximately) linear relationship between σ^2 and ν. For each neuron, this relationship should be characterized by a single constant A. Given a particular value of A, this equation provides us with a second constraint on parameter space. Different values of parameters J, g, and C_E that give the same value of A should give the same firing statistics. Note that this relationship describes a two-dimensional manifold in the three-dimensional (J, g, C_E) parameter space. Does this two-dimensional manifold fit with the one obtained from the fitting procedure? To answer this question, we plotted *Eq. 40* in $g > 4$ region for a fixed value of A (A = 3,025 for Fig. 6*A*, A = 225 for *B*) that fits the global minimum shown as an open circle. Interestingly, this equation obtained from simple balance arguments seems to fit the contours of the cost function very well, especially for $C_E >= 100$. For lower C_E (C_E = 10), the exact balance condition line does not fit the lowest cost region very well. This is consistent with the fact that the analytical argument is obtained in the large C_E limit and therefore cannot be expected to reproduce quantitatively the results of the fitting procedure in the low C_E region. In any case, this analysis shows that, to obtain a certain firing rate and firing irregularity, there are infinite numbers of network architectures with different values of g, J, and C_E, but these parameters are constrained in a specific way.

The constraint on the network parameters can be easily understood from the *Eq. 40*. This equation implies that for a given value of C_E, J is approximately inversely proportional to g. It also implies that when C_E increases, the magnitude of J scales as the square root of C_E ($J \propto 1/\sqrt{C_E}$). Therefore as C_E increases, the low cost region tends to be confined to the lower values of J region. The dependence of the best-fit parameters

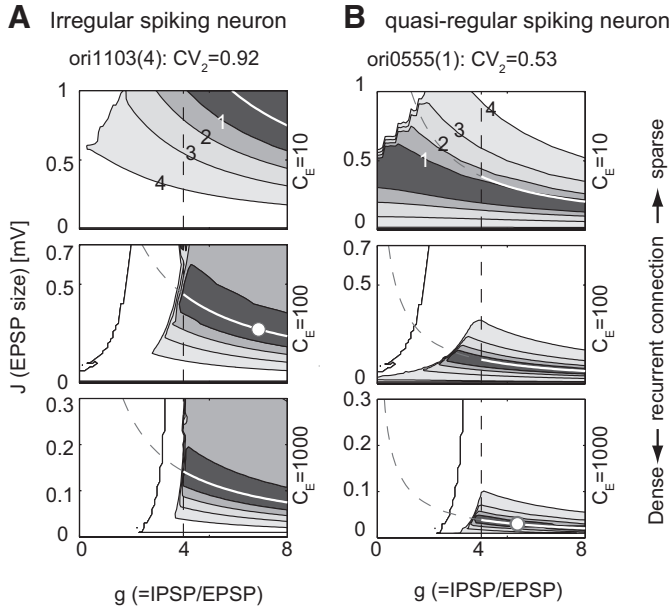

FIG. 6. Contour plot of log(cost) in J-g plane at various sections of C_E = [10, 100, 1,000] from the same neurons as shown in Fig. 5. The contour lines are plotted at log(cost) = {1, 2, 3, 4}. The global minimum is shown by an open circle. The manifold of the exact balance of total excitation and total inhibition [*Eq. 40*, A = 3,025 for A, A = 225 for B, shown in white line in $g >$ 4 region] can well fit the valley of the cost function, suggesting that a specific firing rate-irregularity relationship can be redundantly represented by many different combinations of network parameters. These network parameters are constrained in the following way: When the number of the recurrent connections C_E is large, the lowest cost region is robustly con-fined to the inhibition-dominated region. For more regular spiking neurons, the range of EPSP size J that gives the lowest cost is smaller ($J \sim$ 0.01 mV) than in irregular spiking neurons for a fixed C_E.

Downloaded from jn.physiology.org on May 24, 2011

on the firing irregularity of the neurons can be also easily understood from *Eq. 39*. In general, the higher A, the larger becomes the variance of the input for a given same firing rate. Therefore the higher the constant A, the higher the firing irregularity (CV_2). If two neurons have the same level of EPSP size and IPSP/EPSP ratio but have different levels of firing irregularity, the neuron with the lower CV_2 value should have a smaller recurrent connectivity C_E because the lower the CV_2, the smaller is the constant A.

DISTRIBUTION OF ESTIMATED PARAMETERS OVER THE POPULATION. We focused on two typical neurons in our data set, one irregular, the other more regular. We now show the distribution of the estimated parameters across the population of neurons. To understand how the best-fit parameters are distributed, we plot the parameter that gives a global minimum for each condition in Fig. 7. Estimated parameters are colored based on their mean CV_2 to clarify the relationship between the firing irregularity and the estimated parameters.

When the number of recurrent connections per neuron, C_E, is small ($C_E = 10$), the estimated parameters g for irregular spiking neurons ($CV_2 > 0.9$) are concentrated in the inhibition-dominated region ($g > 4$), but for quasi-regular spiking neurons, parameters providing a good fit extend in both the excitation and inhibition dominated region depending on EPSP size.

When the number of recurrent connections becomes large ($C_E = 100$), the local cortical circuits need to be inhibition dominated networks to account for the dynamics mainly for high CV_2 neurons and the EPSP size J approaches more realistic values ($J \approx 0.2$). For a neuron with a CV_2 lower than 0.6, the estimated balance level (g) distributes mainly in inhibition-dominated but can still be slightly extended to excitation-dominated region. The estimated EPSP size J of quasi-regular neurons tends to be lower than that of irregular spiking neurons.

As the number of recurrent connections becomes large ($C_E = 1{,}000$), the EPSP size becomes smaller for a similar level of spike irregularity, and for almost all the range of irregularity, the estimated balance level is confined to the inhibition-dominated region. For all C_E, 78.5% (322/410) of estimated parameters the cost of which is <5 are classified as locally inhibition-dominated ($g > 4$). This result is consistent with the first constraint (*Eq. 38*) on the parameter space. The conclusion of inhibition-dominance does not change for a different set of single neuron parameters (Supplementary Fig. S4).

EFFECT OF THE SYNAPTIC PROPERTIES ON THE ESTIMATION RESULTS. We found that the landscape of the cost-function is degenerate, but the estimated network parameter is mostly confined in the inhibition-dominated region. The higher CV_2 neurons tend to have larger EPSP size J for a fixed number of presynaptic neurons C_E. The neuron model we have used was the simple current-based LIF neuron that allows us to clearly understand the estimation process. However, real synaptic currents have rich biophysical properties, such as voltage-dependence and short-term plasticity. To understand how our results are affected by incorporating additional biophysical synaptic features to our model, we applied our estimation method to two types of LIF neuron models—with synapses with STD and with conductance-based synapses—and studied their effect on our estimation results.

STD in excitatory synapses. One significant feature of the neocortical neurons is their activity-dependent short-term synaptic plasticity (Thomson et al. 1993). Because short-term plasticity in recurrent synapses nonlinearly modulates the input statistics, its contribution to the firing statistics is not straight forward. Here we used our parameter estimation method to the LIF neuron model with excitatory STD synapses. In the STD model, the average EPSP size is $Ju\langle x\rangle$ where J is the "absolute" synaptic strength, u is the fraction of released vesicles from the available resources, and $\langle x\rangle$ is the average fraction of available vesicles (see METHODS). $\langle x\rangle$ in turn depends on the firing rate of presynaptic neurons and is <0.2 for the parameters chosen here and if the firing rate is more than 10 Hz. Parameter values of $u = 0.5$ and $\langle x\rangle \sim 0.2$ make the effective EPSP amplitude $Ju\langle x\rangle \sim 10$ times smaller than the absolute synaptic strength J. This indicates that, for a synapse with STD to achieve the same EPSP size as a synapse with no STD, the absolute value of EPSP size J must be nearly 10 times larger than that of a synapse with no STD. This also means that the parameter g is no longer a good measure for the balance between excitation and inhibition. This balance is now $g/u\langle x\rangle$, where $\langle x\rangle$ is firing rate dependent. We therefore plotted the best-fit parameters in the $Ju\langle x\rangle - g/u\langle x\rangle$ plane in Fig. 8*A*, as well as in the $Ju - g/u\langle x\rangle$ plane in *B*. For each neuron, we computed $\langle x\rangle$ from its median firing rate. The effective EPSP size during the task can be approximated by $Ju\langle x\rangle$, but we also used Ju, which corresponds to the EPSP size in absence of prior presynaptic activity and is

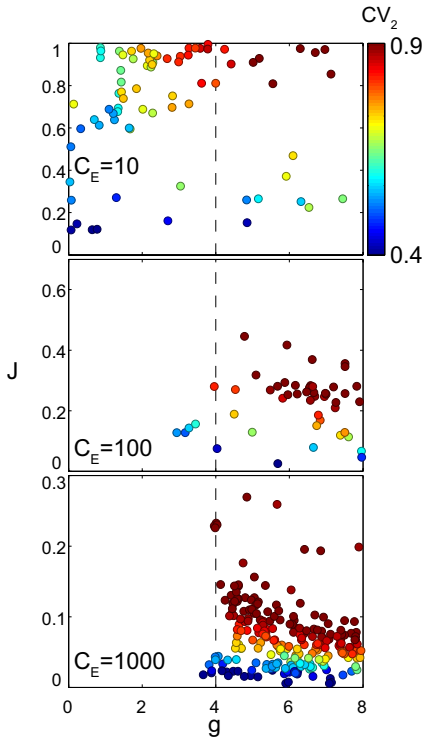

FIG. 7. The global minima in the cost-function of each neuron in 1 condition from both monkeys are plotted in $J-g$ plane at various sections of $C_E = [10, 100, 1{,}000]$. Global minima in $J-g-C_E$ space for 1 specific task condition are plotted. Symbols are color-coded based on the mean CV_2 value of each cell. We analyzed data which satisfied the following criteria; ≥10 data points in time, firing rate changes >10 Hz, and the number of trials is >30. For each task condition of each neuron, we calculated cost(Π) within the 3-dimensional discretized parameter space and find the global minimum.

Downloaded from jn.physiology.org on May 24, 2011

therefore directly comparable to experimental values observed in slice conditions in which neurons are essentially silent.

The distribution of the estimated parameters shows significant differences with the distribution of the estimated parameters in the network with no STD (compare Figs. 7 and 8, *A* and *B*). First, all neurons are no longer confined to the inhibition-dominated region—rather, neurons tends to be now clustered around the balance point. Neurons with high CV_2 still tend to be in the inhibition-dominated region, while many neurons with low CV_2 are in the excitation-dominated region. Second, best-fit parameters tend to have much larger EPSP amplitudes compared with the case with no STD (compare Figs. 7 and 8*B*) due to the fact that in an active network STD reduces the effective EPSP size by a significant factor. A feature that is qualitatively unchanged is that high CV_2 neurons tend to have higher *J*, larger *g* values.

Conductance-based synapses. We turn now to another biophysical property of synapses, the voltage dependence of the synaptic currents. Modeling studies have shown that the LIF neuron model with conductance-based synapses does not require a strict balance between excitation and inhibition (Meffin et al. 2004) to achieve high irregularity of firing. We used conductance-based synapses in LIF neuron models and estimated network parameters for the same set of neuron data (see the parameters in METHODS). The estimated parameters showed a qualitatively similar distribution as the current-based LIF neuron network (Fig. 8*C*). The estimated parameters are shown in the effective EPSP size $[a_E(V_r - V_E)]$ and the effective ratio of IPSP to EPSP $[g = (a_I|V_r - V_I|)/a_E(V_r - V_E)]$ measured at the reset potential V_r. The high CV_2 neurons tend to have higher effective EPSP values and higher *g* values for a fixed C_E. Therefore our estimation results are consistent in both the current- and conductance-based models. In Fig. 8*D,* we also showed the distribution of the effective time constants of each neuron computed from its median firing rate. The high CV_2 neurons tend to have lower effective membrane time constant (compare Fig. 8, *C* and *D*) because they have larger EPSP and IPSP sizes (see *Eq. 33*), and given that there is no significant correlation between mean firing rate and CV_2 (Fig. 4*F*).

Stochastic synapses. Another prominent property of synapses is the variability of the amplitude of postsynaptic potentials from spike to spike. This variability can be quantified by the CV (SD divided by the mean). For connections between cortical pyramidal cells, the CV is typically of order 0.5 (Markram et al. 1997). How does this variability affect our results? It turns out that we can answer this question in a very

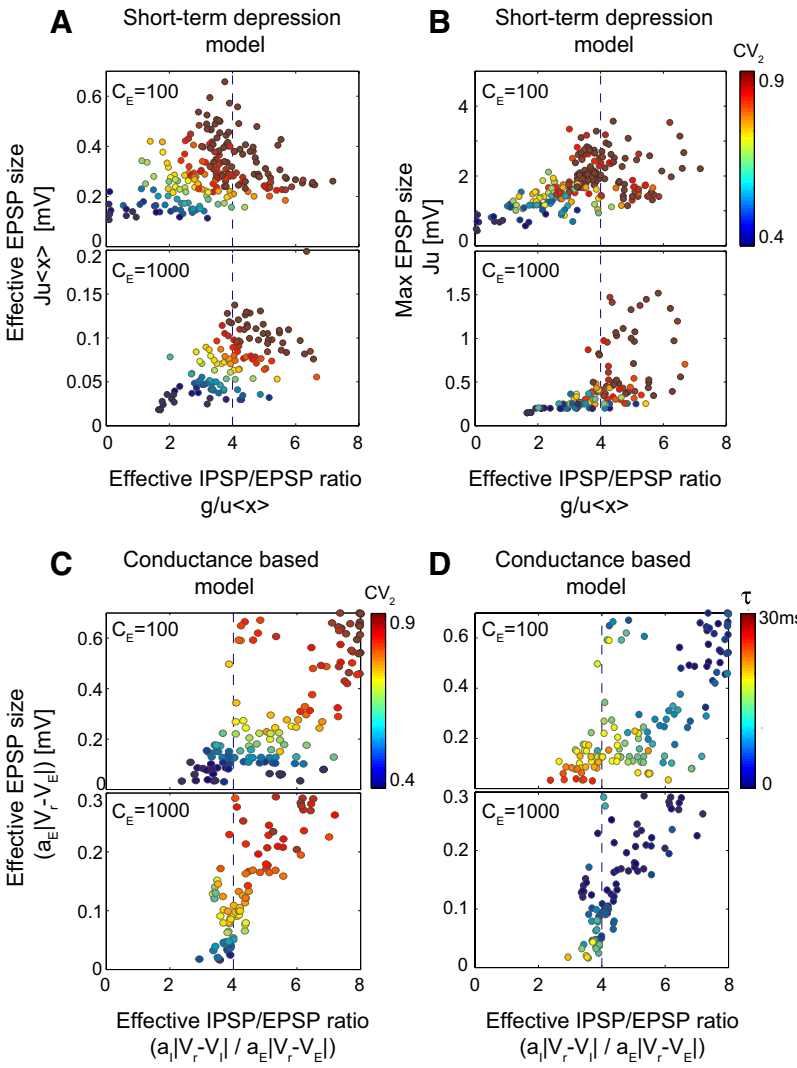

FIG. 8. The global minima in the cost-function of each neuron in one condition from both monkeys are plotted by using (*A* and *B*) the short-term depression (STD) based model or (*C* and *D*) the conductance-based model. *A* and *B*: the distribution of global minima are plotted with the average balance ($g/u\langle x\rangle$) in the *x* axis vs. the effective EPSP size ($Ju\langle x\rangle$) in *A* and the maximum EPSP size (Ju) in *B* in the *y* axis, for a fixed C_E = [100, 1,000]. Symbols are color-coded based on the mean CV_2 value of each cell. *C* and *D*: the distribution of global minima are plotted in effective EPSP size ($a_E|V_r - V_E|$)—effective balance ($a_I|V_r - V_I|/a_E|V_r - V_E|$) coordinates for the fixed C_E = [100, 1,000]. Symbols are color-coded based on the mean CV_2 value (*C*) or the mean effective time constant τ (*D*) of the cell. Data selection criteria are the same as described in Fig. 7.

Downloaded from jn.physiology.org on May 24, 2011

simple way, by evaluating how the variability affects the variance of the fluctuations due to random synaptic inputs. With stochastic synapses, the variance becomes

$$\sigma^2 = cJ^2(1 + CV_{syn}^2)(\nu'_{ext} + C_E\nu(1 + g^2\beta))$$

where CV_{syn} is the CV of PSPs, which is assumed here for simplicity to be the same for all types of synapses. The next question is the impact of this variability on the best-fit parameters. This question can be answered by inspecting *Eq. 40*. To satisfy this equation for a given value of A, we see that an increase in CV_{syn} should lead to a corresponding decrease in J and/or g. In the case of g, the constraint $g > 1/\beta$ still holds, so g cannot be decreased below this value. In practice, for realistic values of $CV_{syn} \sim 0.5$, the decrease in typical PSP strengths is small ($\sim$10%).

Finite synaptic decay times. In the model studied here, postsynaptic currents are assumed to be delta functions. Including a finite decay time of postsynaptic currents complicates significantly the calculation of both firing rates and CV of the ISIs as a function of the statistics of the input. In fact, only expressions in the limit in which synaptic decay time is either very short or very large compared with the membrane time constant are known (see e.g., Brunel and Sergi 1998; Fourcaud and Brunel 2002; Moreno et al. 2002). However, we can understand the qualitative effect of such time constants by looking at the results of these previous studies. In practice, incorporating a finite decay time constant leads to an effective decrease in the SD of the noise (see e.g., Fourcaud and Brunel 2002). So the result of incorporating a synaptic decay time constant should be the opposite of incorporating stochasticity of synaptic transmission. For example, for a fixed value of g and C_E, the estimated EPSP amplitude J should increase as the synaptic decay time constant increases.

DISCUSSION

In this paper, we analyzed single-unit recordings from motor cortex of two behaving monkeys. These data show two interesting features of the firing statistics of these neurons: in many neurons, the firing irregularity, as measured by CV_2, fluctuates very little in time and across task conditions even though the firing rates exhibit pronounced modulations and the distribution of the CV_2 values of all cells is rather broad, ranging from 0.3 to >1. We then explored what a specific temporal rate-CV_2 relationship tells us about the structure of the local network in which the neuron is embedded. We introduced a method to find the parameters of a randomly connected network of excitatory and inhibitory LIF neurons that minimize the distance between data and model. This method indicates that most recorded cells in motor cortex live in local networks that are dominated by inhibition when considering a simple current-based model. This result can be understood with the following intuitive argument: if rate modulations are simply due to changes in external excitatory inputs, then one would expect that the CV_2 decreases monotonically with rate. This is because when the external inputs are low, firing occurs due to fluctuations in the inputs and is approximately Poisson with a CV_2 close to 1. On the other hand, when the external inputs are high, firing becomes more deterministic with a CV_2 that decreases with input strength. In fact, in cortical slices, the CV of both pyramidal cells and interneurons decreases monotonically with the mean injected current, when the variance of the noise is fixed (La Camera et al. 2006; Rauch et al. 2003). This argument no longer holds true in networks dominated by inhibition because the increase in external inputs tends to be counterbalanced by an increase in the firing rate of inhibitory neurons. In such networks, an increase in firing rate can be induced by a combination of an increase in the mean inputs and an increase in the variance of the fluctuations (see also Renart et al. 2006). Whereas the increase in the mean inputs tends to decrease the CV_2, the increase in the variance has the opposite effect of decreasing the CV_2. Therefore there exists a combination of the two effects that leads to an approximately constant firing irregularity as the rate changes (Miura et al. 2007).

Weak modulation in firing irregularity

High irregularity is a hallmark of electrophysiological recordings in cortex in vivo (Compte et al. 2003; Shinomoto et al. 2003; Softky and Koch 1993). Shimokawa and Shinomoto (2009) have studied the instantaneous firing irregularity based on Bayesian estimation and concluded that the firing irregularity fluctuates only weakly for neurons in cortical areas V1 and MT compared with those in the LGN of the thalamus. Here we also find that the CV_2 is approximately constant for most cells throughout the whole trial. Our estimation method then suggests this weak modulation in firing irregularity could be due to recurrent dynamics of a local network dominated by inhibition. This is consistent with a recent in vitro study that showed that a balanced input can decouple the firing rate from the firing irregularity (Miura et al. 2007). In other words, when the excitatory and inhibitory conductances are proportionally changed, firing irregularity can be fixed but the firing rate can be modulated independently (see also Ponce-Alvarez et al. 2010).

There are, however, alternative explanations to the weakly modulated irregularity. Barbieri and Brunel (2007) showed that the CV of a simple LIF neuron becomes weakly dependent on the rate in a wide range of rates when the reset potential is very close to threshold and the membrane time constant is short. With these parameter settings, an approximately constant CV could be explained by single cell properties, rather than by network properties. The CV versus rate relationship of cortical cells measured in vitro shows, however, a pronounced decrease of CV as a function of rate, which seems at odds with the single cell scenario (La Camera et al. 2006; Rauch et al. 2003).

Wide distribution of irregularity measures

The results of our analysis suggest that the distribution of the CV_2 is wide, ranging from 0.3 to >1. This is consistent with the analysis of spiking activities recorded in other areas (Shinomoto et al. 2003, 2005, 2009). Again, one might think about two possible explanations to account for this wide distribution; network or single cell. If all recorded cells have the same characteristics, our analysis suggests that there is a wide range of coupling strengths in local networks of motor cortex and that neurons with low CV_2 could be part of networks that are relatively weakly coupled (either with small numbers of recurrent connections per neuron or with very weak EPSP/IPSP amplitudes). Another "network" explanation is provided by Shinomoto et al. (2005), who showed that in area TE layer V–VI neurons tend to have a lower firing irregularity than layer

Downloaded from jn.physiology.org on May 24, 2011

II–III neurons. In both scenarios, the network connectivity would be the source of the observed wide distribution of firing irregularities. Another possibility is that there are several classes of neurons with distinct intrinsic properties, each of which being characterized by a distinct CV.

Comparison of best-fit parameters with estimates from the literature

Our method provides constraints on parameters characterizing the network architecture: J (the EPSP size), C_E (the number of excitatory recurrent connections per neuron), and g (the IPSP/EPSP ratio). The strongest constraint is on g: our method predicts that for most recorded neurons, $g > 4$ (inhibition dominance) when using a simple current-based model. The second constraint can give us an upper bound on J given a particular value of C_E. The next question is whether the best-fit parameters are compatible with known experimental data?

The most robust finding of our estimation method is that the IPSP to EPSP ratio should be large enough to compensate for the fact that there are less inhibitory neurons than (excitatory) pyramidal neurons in cortex. This is in agreement with the fact that inhibitory synapses are located mainly on the cell body and, thus the size of their synaptic potential is less attenuated than that of excitatory synapses that are mainly located on the dendrites (Braitenberg and Schüz 1998). Furthermore, in our network interneurons are constrained to have the same firing rate as pyramidal cells. If interneurons have higher firing rates (La Camera et al. 2006; McCormick et al. 1985; Wilson et al. 1994), then the constraint on g can be alleviated (Amit and Brunel 1997). Incorporating STD, however, leads to a large number of neurons (especially the low CV ones) to move to the excitation-dominated region.

Our estimate of the EPSP size depends strongly on the number, C_E, of excitatory recurrent connections per neurons and is not very constrained. This is because for a fixed IPSP to EPSP ratio, the same firing rate and firing irregularity can be achieved for widely different values of J and C_E, provided *Eq. 40* is satisfied. In a model with no synaptic STD, for realistic values of C_E ($\geq$1,000) (Braitenberg and Schüz 1998), our average EPSP sizes are typically small, on the order of 0.1- 0.2 mV, for high CV neurons, and even smaller ($<$0.1 mV) for low CV neurons (see Fig. 7). Inserting STD in the model leads to much higher EPSP sizes because STD leads to strong decrease of the effective EPSP size. In vitro studies reported average EPSP sizes in the range [0.1–1 mV] in neocortex (Holmgren et al. 2003; Markram et al. 1997; Mason et al. 1991; Sjöström et al. 2001). EPSP sizes have been reported to be in the order of 0.1–0.6 mV in monkey motor cortex in vivo (Matsumura et al. 1996). These numbers are consistent with our estimates provided STD is included in the model.

We have investigated a network of LIF neurons because of analytical tractability. Interestingly, both the *f-I* curve and *CV-I* curve of cortical pyramidal cells can be well fitted by the corresponding curves of integrate-and-fire neurons in vitro (Rauch et al. 2003). Exponential integrate-and-fire (EIF) neurons (Fourcaud-Trocmé et al. 2003) have been shown to provide a better fit of the timing of spikes of cortical pyramidal cells on injection of random fluctuating inputs (Badel et al. 2008), but both the *f-I* curve and *CV-I* curve of EIF neurons are qualitatively similar to those of LIF neurons (Fourcaud-Trocmé et al. 2003; Brunel, unpublished observations), so we would not expect any qualitative difference between LIF and EIF neurons as far as the results reported here are concerned.

Functional implications

The surprising result that a high proportion of the analyzed neurons from motor cortex of the behaving monkey seem to be embedded in a network dominated by inhibition is in agreement with the notion that during movement preparation (neuronal activity was recorded mainly during movement preparation) the corticospinal motor output must be inhibited to prevent its premature recruitment. This preparatory activity goes in line with a wide spread oscillatory activity in the beta range of the LFP in motor cortical areas (MacKay 2005; Murthy and Fetz 1992), which stops abruptly with movement onset. Interestingly, delay-related oscillatory activity is often associated with an inhibitory behavior as well as expectancy, an activity that closely corresponds to the withholding of the movement during the delay period (for a review, see MacKay 2005; see also Riehle et al. 2006). It is only at the end of the delay that the inhibition of corticospinal neurons would be lifted and a local wave of excitatory input would briskly ignite a descending motor volley, corresponding to the small networks of rather regular spiking neurons.

ACKNOWLEDGMENTS

Data were collected in the lab of A. Riehle mainly by Sébastien Roux and Franck Grammont. We thank M. Martin for animal care, B. E. Kilavik and A. Ponce-Alvarez for many helpful discussions; and G. Mongillo for clarifications about the short-term depression model.

Present address of K. Hamaguchi: Mooney Lab, Bryan Research Bld., Duke University Medical Center, Research Dr., Durham, NC 27710.

GRANTS

K. Hamaguchi was supported by Japan Society for the Promotion of Science Research Fellowship for Young Scientists. A. Riehle and N. Brunel were supported by the French Government (ANR-NEUR-05-045-01).

DISCLOSURES

No conflicts of interest, financial or otherwise, are declared by the author(s).

REFERENCES

Abramowitz M, Stegun IA. *Tables of Mathematical Functions*. New York: Dover, 1970.

Amit DJ, Brunel N. Model of global spontaneous activity and local structured activity during delay periods in the cerebral cortex. *Cereb Cortex* 7: 237–252, 1997.

Arsiero M, Lüscher H-R, Lundstrom BN, Giugliano M. The Impact of input fluctuations on the frequency-current relationships of layer 5 pyramidal neurons in the rat medial prefrontal cortex. *J Neurosci* 27: 3274–3284, 2007.

Badel L, Lefort S, Brette R, Petersen CC, Gerstner W, Richardson MJ. Dynamic *I-V* curves are reliable predictors of naturalistic pyramidal-neuron voltage traces. *J Neurophysiol* 99: 656–666, 2008.

Barbieri F, Brunel N. Irregular persistent activity induced by synaptic excitatory feedback. *Front Comp Neurosci* 1: 5, 2007.

Braitenberg V, Schüz A. *Anatomy of the cortex. Statistics and Geometry*. Berlin: Springer, 1998.

Brunel N. Dynamics of sparsely connected networks of excitatory and inhibitory spiking neurons. *J Comp Neurosci* 8: 183–208, 2000.

Brunel N, Sergi S. Firing frequency of leaky intergrate-and-fire neurons with synaptic current dynamics. *J Theor Bio* 195: 87–95, 1998.

Burkitt AN. Balanced neurons: analysis of leaky integrate-and-fire neurons with reversal potentials. *Biol Cybern* 85: 247–255, 2001.

Downloaded from jn.physiology.org on May 24, 2011

Compte A, Constantinidis C, Tegner J, Raghavachari S, Chafee MV, Goldman-Rakic PS, Wang XJ. Temporally irregular mnemonic persistent activity in prefrontal neurons of monkeys during a delayed response task. *J Neurophysiol* 90: 3441–3454, 2003.

Daniels HE. Exact saddlepoint approximations. *Biometrika* 67: 59–63, 1980.

Davies RM, Gerstein GL, Baker SN. Measurement of time-dependent changes in the irregularity of neural spiking. *J Neurophysiol* 96: 906–918, 2006.

Fourcaud N, Brunel N. Dynamics of the firing probability of noisy integrate-and fire neurons. *Neural Comp* 14: 2057–2110, 2002.

Fourcaud-Trocmé N, Hansel D, van Vreeswijk C, Brunel N. How spike generation mechanisms determine the neuronal response to fluctuating inputs. *J Neurosci* 23: 11628–11640, 2003.

Gerstein GL, Mandelbrot B. Random walk models for the spike activity of a single neuron. *Biophys J* 4: 41–68, 1964.

Green DM, Swets JA. *Signal Detection Theory and Psychophysics*. New York: Wiley, 1966.

Haider B, Duque A, Hasenstaub AR, McCormick DA. Neocortical network activity in vivo is generated through a dynamic balance of excitation and inhibition. *J Neurosci* 26: 4535–4545, 2006.

Hamaguchi K, Riehle A, Brunel N. *A method to estimate statistical properties of input currents and network structure from dynamics of rate and spike irregularity. Computational and Systems Neuroscience 2008 (Cosyne 2008)*, Salt Lake City, UT, 2008.

Hodgkin AL, Huxley AF. A quantitative description of membrane current and its application to conduction and excitation in nerve. *J Physiol* 117: 500–544, 1952.

Holmgren C, Harkany T, Svennenfors B, Zilberter Y. Pyramidal cell communication within local networks in layer 2/3 of rat neocortex. *J Physiol* 551: 139–153, 2003.

Holt GR, Softky WR, Koch C, Douglas RJ. Comparison of discharge variability in vitro and in vivo in cat visual cortex neurons. *J Neurophysiol* 75: 1806–1814, 1996.

Koch C. *Biophysics of Computation*. Oxford, UK: Oxford Univ. Press, 1999.

La Camera G, Rauch A, Thurbon D, Lüscher H-R, Senn W, Fusi S. Multiple time scales of temporal response in pyramidal and fast spiking cortical neurons. *J Neurophysiol* 96: 3448–3464, 2006.

MacKay WA. Wheels of motion: oscillatory potentials in the motor cortex. In: *Motor Cortex in Voluntary Movements: A Distributed System for Distributed Functions*, edited by Riehle A, Vaadia E. Boca Raton, FL: CRC, 2005, p. 181–211.

Maimon G, Assad JA. Beyond Poisson: Increased spike-time regularity across primate parietal cortex. *Neuron* 62: 426–440, 2009.

Markram H, Lübke J, Frotscher M, Roth A, Sakmann B. Physiology and anatomy of synaptic connections between thick tufted pyramidal neurones in the developing rat neocortex. *J Physiol* 500: 409–440, 1997.

Mason A, Nicoll A, Stratford K. Synaptic transmission between individual pyramidal neurons of the rat visual cortex in vitro. *J Neurosci* 11: 72–84, 1991.

Matsumura M, Chen DF, Sawaguchi T, Kubota K, Fetz EE. Synaptic interactions between primate precentral cortex neurons revealed by spike-triggered averaging of intracellular membrane potentials in vivo. *J Neurosci* 16: 7757–7767, 1996.

McCormick DA, Connors BW, Lighthall JW, Prince DA. Comparative electrophysiology of pyramidal and sparsely spiny stellate neurons of the neocortex. *J Neurophysiol* 54: 782–806, 1985.

Meffin H, Burkitt AN, Grayden DB. An analytical model for the large, fluctuating synaptic conductance state typical of neocortical neurons in vivo. *J Comput Neurosci* 16: 159–175, 2004.

Miura K, Okada M, Amari S-I. Estimating spiking irregularities under changing environments. *Neural Comp* 18: 2359–2386, 2006.

Miura K, Tsubo Y, Okada M, Fukai T. Balanced excitatory and inhibitory inputs to cortical neurons decouple firing irregularity from rate modulations. *J Neurosci* 27: 13802–13812, 2007.

Moreno R, de la Rocha J, Renart A, Parga N. Response of spiking neurons to correlated inputs. *Phys Rev Lett* 89: 288101–4, 2002.

Murthy VN, Fetz EE. Coherent 25- to 35-Hz oscillations in the sensorimotor cortex of bahaving monkeys. *Proc Natl Acad Sci USA* 89: 5670–5674, 1992.

Nawrot MP, Boucsein C, Rodriguez-Molina V, Riehle A, Aertsen A, Rotter S. Measurement of variability dynamics in cortical spike trains. *J Neurosci Methods* 169: 374–390, 2008.

Ponce-Alvarez A, Kilavik BE, Riehle A. Comparison of local measures of spike time irregularity and the use of the optimal measure to relate firing rate and variability in motor cortical neurons. *J Comput Neurosci* 29: 351–365, 2010.

Rauch A, Camera GL, Lüscher H-R, Senn W, Fusi S. Neocortical pyramidal cells respond as integrate-and-fire neurons to in vivo-like input currents. *J Neurophysiol* 90: 1598–1612, 2003.

Renart A, Moreno-Bote R, Wang X-J, Parga N. Mean-driven and fluctuation-driven persistent activity in recurrent networks. *Neural Comp* 19: 1–46, 2006.

Riehle A, Grammont F, MacKay WA. Cancellation of a planned movement in monkey motor cortex. *Neuroreport* 17: 281–285, 2006.

Romani S, Amit D, Mongillo G. Mean-field analysis of selective persistent activity in presence of short-term synaptic depression. *J Comput Neurosci* 20: 201–217, 2006.

Roux S, Coulmance M, Riehle A. Context-related representation of timing processing in monkey motor cortex. *Eur J Neurosci* 18: 1011–1016, 2003.

Roux S, Mackay WA, Riehle A. The pre-movement component of motor cortical local field potentials reflects the level of expectancy. *Behav Brain Res* 169: 335–351, 2006.

Shadlen MN, Newsome WT. The variable discharge of cortical neurons: implications for connectivity, computation and information coding. *J Neurosci* 18: 3870–3896, 1998.

Shimokawa T, Shinomoto S. Estimating irregularity of neuronal firing. *Neural Comp* 21: 1931–1951, 2009.

Shinomoto S, Kim H, Shimokawa T, Matsuno N, Funahashi S, Shima K, Fujita I, Tamura H, Doi T, Kawano K, Inaba N, Fukushima K, Kurkin S, Kurata K, Taira M, Tsutsui K-I, Komatsu H, Ogawa T, Koida K, Tanji J, Toyama K. Relating neuronal firing patterns to functional differentiation of cerebral cortex. *PLoS Comput Biol* 5: e1000433, 2009.

Shinomoto S, Miyazaki Y, Tamura H, Fujita I. Regional and laminar differences in in vivo firing patterns of primate cortical neurons. *J Neurophysiol* 94: 567–575, 2005.

Shinomoto S, Shima K, Tanji J. Differences in spiking patterns among cortical neurons. *Neural Comp* 15: 2823–2842, 2003.

Shu Y, Hasenstaub A, McCormick DA. Turning on and off recurrent balanced cortical activity. *Nature* 423: 288–293, 2003.

Siegert AJF. On the first passage time probability problem. *Phys Rev* 81: 617–623, 1951.

Sjöström PJ, Turrigiano GG, Nelson SB. Rate, timing, and cooperativity jointly determine cortical synaptic plasticity. *Neuron* 32: 1149–1164, 2001.

Softky WR, Koch C. The highly irregular firing of cortical cells is inconsistent with temporal integration of random EPSPs. *J Neurosci* 13: 334–350, 1993.

Sugiyama H, Moore GP, Perkel DH. Solution of a stochastic model of neuronal spike production. *Math Biosci* 8: 323–341, 1970.

Thomson AM, Deuchars J, West DC. Large, deep layer pyramid-pyramid single axon EPSPs in slices of rat motor cortex display paired pulse and frequency-dependent depression, mediated presynaptically and self-facilitation, mediated postsynaptically. *J Neurophysiol* 70: 2354–2369, 1993.

Tsodyks M, Markram H. The neural code between neocortical pyramidal neurons depends on neurotransmitter release probability. *Proc Natl Acad Sci USA* 94: 719–723, 1997.

Tsodyks M, Sejnowski TJ. Rapid state switching in balanced cortical network models. *Network: Comput Neural Syst*: 111–124, 1995.

Tuckwell H. *Introduction to Theoretical Neurobiology*. Cambridge, UK: Cambridge Univ. Press, 1988.

van Vreeswijk C, Sompolinsky H. Chaos in neuronal networks with balanced excitatory and inhibitory activity. *Science* 274: 1724–1726, 1996.

van Vreeswijk C, Sompolinsky H. Chaotic balanced state in a model of cortical circuits. *Neural Comp* 10: 1321–1372, 1998.

Varela JA, Sen K, Gibson J, Fost J, Abbott LF, Nelson SB. A quantitative description of short-term plasticity at excitatory synapses in layer 2/3 of rat primary visual cortex. *J Neurosci* 17: 7926–7940, 1997.

Wilson FA, O'Scalaidhe SP, Goldman-Rakic PS. Functional synergism between putative gamma-aminobutyrate-containing neurons and pyramidal neurons in prefrontal cortex. *Proc Natl Acad Sci USA* 91: 4009–4013, 1994.

Downloaded from jn.physiology.org on May 24, 2011